Security Authentication with a Three-Dimensional Optical Phase Code Using Random Forest Classifier

ADAM MARKMAN,[1] ARTUR CARNICER,[2] BAHRAM JAVIDI[1,*]

[1] *Electrical and Computer Engineering Department, University of Connecticut, 371 Fairfield Road, Storrs, Connecticut 06269, USA*
[2] *Universitat de Barcelona (UB), Facultat de Física, Departament de Física Aplicada i Òptica, Martí i Franquès 1, 08028 Barcelona, Spain*
**Corresponding author: bahram@engr.uconn.edu*

Received XX Month XXXX; revised XX Month, XXXX; accepted XX Month XXXX; posted XX Month XXXX (Doc. ID XXXXX); published XX Month XXXX

An object with a unique three-dimensional (3D) optical phase mask attached is analyzed for security and authentication. These 3D optical phase masks are more difficult to duplicate or to have a mathematical formulation compared with 2D masks, and thus have improved security capabilities. A quick response code was modulated using a random 3D optical phase mask generating a 3D optical phase code (OPC). Due to the scattering of light through the 3D OPC, a unique speckle pattern based on the materials and structure in the 3D optical phase mask is generated and recorded on a CCD device. Feature extraction is performed by calculating the mean, variance, skewness, kurtosis, and entropy for each recorded speckle pattern. The random forest classifier is used for authentication. Optical experiments demonstrate the feasibility of the authentication scheme.

OCIS codes: *(100.4993) Pattern recognition, optical security and encryption, (030.6140) Speckle; (110.0110) Imaging systems;*

http://dx.doi.org/10.1364/AO.99.099999

1. Introduction

Optical information security has sought to ensure the secure transmission of an image to a recipient. This area of research includes image encryption [1-15], authentication [16-24], and compression or secure storage [25, 26]. Authenticating sensitive information is critical to discovering tampering caused by a miscreant. Methodologies for image authentication includes both optical [16-21] and simulated [22, 23] authentication schemes.

Recently, authentication schemes have been investigated using optically tagged security codes [19-21]. In these authentication schemes, an object is optically tagged using a phase mask. In [19], these phase masks were as simple as Scotch tape. In [20], optical codes based on thin-film technology were produced for security applications. These structures generate distinctive polarimetric information that can be utilized to authenticate the message encoded. In [21], more complex phase masks consisted of embedding nanoparticle structures such as gold in an object. An optical set up was then used to authenticate objects containing the phase mask by illuminating the object with a laser diode. The polarimetric information from the object was recorded and used for authentication. In [16], an authentication scheme using a three-dimensional (3D) phase object was created by illuminating a 3D phase object with two different wavelengths and recording the resulting speckle pattern with a CCD device. These speckle patterns were then correlated with authentic speckle patterns from a database to verify the veracity of the 3D phase object.

In this work, we propose a 3D optical phase code (OPC) by encoding a quick response (QR) code with a 3D optical phase mask. An advantage of using a 3D optical phase mask compared with a 2D mask is its difficulty in being duplicated by simple examination of the optical phase mask or the resulting speckle pattern. The 3D optical phase mask may be generated in a variety of methods. In our experiments, it consists of a combination of glass slides and diffuser material. A 445 nm wavelength blue laser diode is transmitted through the 3D OPC generating a unique speckle pattern that is recorded on a CCD. From the recorded speckle pattern, the mean, variance, skewness, kurtosis, and entropy is computed. The random forest classifier is then used to authenticate the phase masks.

2. 3D Optical Phase Code Design and Feature Selection

Three-dimensional OPCs were created as shown in Fig. 1. A 4 mm × 4 mm QR code was first printed on transparency paper. A 3D optical phase mask was then placed on the QR code. In the experiment, three phase mask configurations were used. As shown in Fig. 1(a), a glass slide and diffuser paper were placed on a QR code; we denote this configuration as 3D OPC A. Figure 1(b) depicts a glass slide and diffuser paper along with an additional glass slide and diffuser paper placed on a QR code; we denote this configuration as 3D OPC B. Lastly, Fig. 1(c) depicts a glass slide and diffuser paper along with an additional glass slide, diffuser paper, and glass slide placed on a QR code, generating 3D OPC C. We note that phase codes were held together by Scotch tape; however we verified that the tape was placed sufficiently far from the QR code. Thus, when illuminated by a laser source, the laser would not be transmitted through the tape. Fig. 2(a) shows the experimental 4 mm × 4 mm QR code used while Fig. 2(b) depicts 3D OPC A. The 3D OPCs generate a highly nonlinear scattering of light due to being an inhomogeneous material [27-30]. In addition, the light transmitted

through the 3D OPCs cannot be easily described with conventional wave propagation models [31]. This highly nonlinear light propagation, though difficult to model, can be used as a unique phase mask. Having this complex phase mask is ideal to serve as an optical tag to create a unique signature for an object.

Once the 3D optical phase codes were developed, an optical experiment was carried out as shown in Fig. 3. A 3D OPC was placed on a translation stage. A blue laser diode having a wavelength of 445 nm was transmitted through first a polarizer to lower the intensity followed by a lens to expand the light. The light was then transmitted through the 3D OPC. A Canon EOS 600D with a CCD sensor size of 14.9 mm (v) × 22.3 mm (w) was used to record the resulting speckle pattern which was 2784 (v) × 1856 (w) pixels. Twenty speckle patterns were recorded for when the 3D OPC was 30 mm, 70 mm, 110 mm, and 150 mm from the CCD sensor. Note that the statistical properties of a speckle, which is a nonstationary process, can be influenced by environmental effects including vibrations [31].

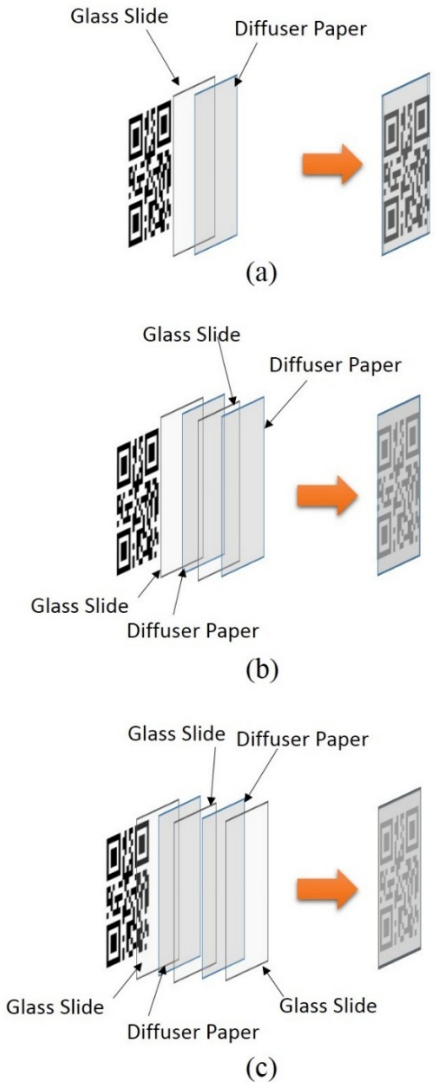

Fig. 1. Workflow for developing the 3D optical phase code for (a) 3D optical phase code A, (b) 3D optical phase code B, and (c) 3D optical phase code C.

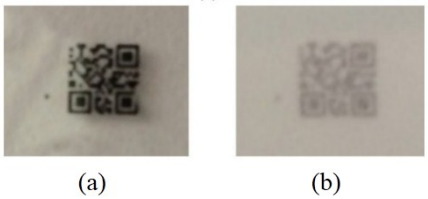

Fig. 2. (a) Experimental 4 mm × 4 mm QR code and a picture of (b) 3D optical phase code A, which consists of a QR code with an optical phase mask consisting of a glass slide and diffuser paper.

A CCD is an intensity recording device and the recorded speckle patterns can be approximated as a statistical distribution. It can be shown that the statistical pattern can be approximated as a Gamma distribution [32]:

$$\Gamma(I)=\left(\frac{n_0}{\bar{I}}\right)^{n_0}\frac{\Gamma^{n_0-1}\exp\left(-In_0/\bar{I}\right)}{\Gamma(n_o)} \qquad n_o=\left(\frac{\bar{I}}{\sigma}\right)^2, \qquad \textbf{(1)}$$

where I, $\bar{I}$, and σ are the intensity data points, its average and the corresponding standard deviation, respectively.

An example of the speckle patterns captured is shown in Fig. 4 for a distance, d, of 110 mm from the CCD using 3D OPCs A, B and C, respectively, along with their corresponding histograms. We note that the color map was adjusted to improve the visualization of the speckle. Using Eq. 1, a gamma distribution was also fitted to the histograms. The images were normalized to lie between the interval [0, 1].

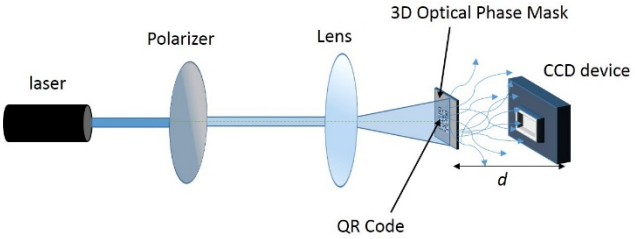

Fig. 3. Optical experimental setup. A 455 nm blue laser diode is transmitted through a polarizer and lens. The laser is then transmitted through the QR code which has a 3D optical phase mask placed on it. A CCD sensor, a distance *d* away from the QR code, records the speckle pattern.

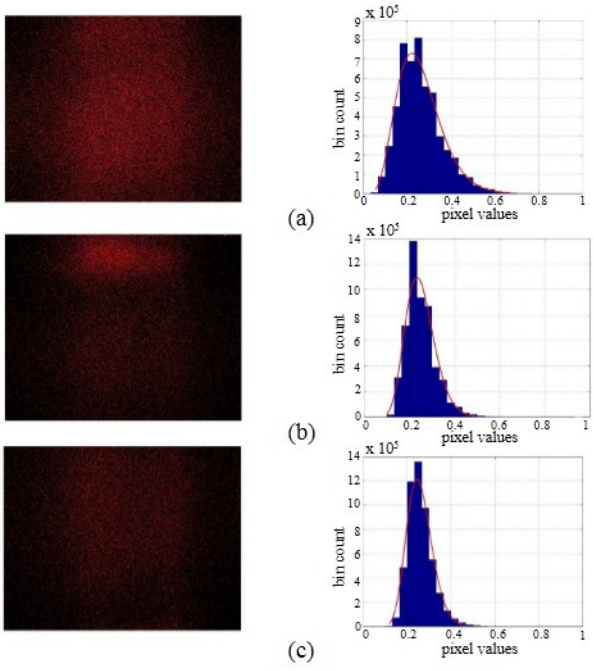

Fig. 4. (a,b,c) The speckle patterns obtained using 3D optical phase codes A, B, and C, respectively. The 3D optical phase codes are a distance of 110 mm from the CCD sensor. The corresponding histograms and a fitted Gamma distribution are also shown.

In our proposed authentication scheme, we extract statistical features from each speckle pattern to be used for classification. The chosen features were: mean, variance, skewness, kurtosis, and entropy. The skewness and kurtosis can be used to examine the location and variability of a distribution, respectively [33]. The skewness measures the third moment of a distribution and measures the symmetry of a distribution. Since the speckle patterns are unimodal, negative skewness values mean the left tail is longer than the right tail of the distribution. Moreover, a positive skewness indicates the right tail is longer than the left tail. The kurtosis measures the fourth moment of a distribution and describes the curvature of the distribution. This metric measures how much the data is peaked or flat relative to a standard normal distribution. For feature extraction, the unbiased skewness and kurtosis was used [34]. Lastly, the entropy [35, 36] measures the average uncertainty, or variability, of an image. The minimum uncertainty occurs at an entropy of 0. The mean, unbiased variance, skewness and kurtosis along with the entropy are defined as:

$$\hat{\mu} = \frac{1}{N}\sum_{i=1}^{N} x_i, \tag{1}$$

$$\hat{\sigma}^2 = \frac{1}{N-1}\sum_{i=1}^{N}\left(x_i - \hat{\mu}\right)^2, \tag{2}$$

$$\hat{s} = \frac{\sqrt{N(N-1)}}{N-2}\frac{\frac{1}{N}\sum_{i=1}^{N}\left(x_i-\hat{\mu}\right)^3}{\left(\sqrt{\frac{1}{N}\sum_{i=1}^{N}\left(x_i-\hat{\mu}\right)^2}\right)^3}, \tag{3}$$

$$\hat{k} = 3 + \frac{N-1}{(N-2)(N-3)}\times \left((N+1)\left[\frac{\frac{1}{N}\sum_{i=1}^{N}\left(x_i-\hat{\mu}\right)^4}{\left(\sqrt{\frac{1}{N}\sum_{i=1}^{N}\left(x_i-\hat{\mu}\right)^2}\right)^4}\right] - 3(N-1)\right), \tag{4}$$

$$H = -\sum_{i=1}^{N} p(x_i)\log_2 p(x_i), \tag{5}$$

where $\hat{\mu}$ is the sample mean, $\hat{\sigma}^2$ is the unbiased sample variance, $\hat{s}$ is the unbiased skewness, $\hat{k}$ is the unbiased kurtosis, H is the entropy, $p(x_i)$ denotes the probability mass function of x_i found by using the relative frequency distribution [37], and N is the total number of pixels,.

By calculating the mean, variance, skewness, kurtosis, and entropy, pixel intensities no longer need to be stored; the only information needed are the five feature values and the classification model. An example of the features extracted at distances of 70 mm and 110 mm are shown in Table 1.

Table 1. Example of mean, variance, skewness, kurtosis, and entropy calculated for recorded speckle patterns

	3D Opitical Phase Code	$\hat{\mu}$	$\hat{\sigma}^2$	$\hat{s}^2$	$\hat{k}$	H
	A	0.099	0.037	0.7142	3.815	5.496
d=70 mm	B	0.087	0.085	0.6202	3.629	4.958
	C	0.106	0.073	0.7013	3.810	4.862
	A	0.070	0.030	0.9297	4.313	5.678
d=110 mm	B	0.070	0.062	1.0310	4.982	4.682
	C	0.065	0.059	1.1067	5.598	4.297

3. 3D Optical Phase Code Authentication Scheme

We chose to use the random forest (RF) classifier [38, 39] for the classification model. This supervised, non-parametric classifier has reduced variance and is robust to overfitting. In essence, the random forest combines the outputs of many independent decision trees, which is a type of binary tree that contains nodes, branches, and leaves. A "vote" is made by averaging the final results of each decision and the majority vote indicates the predicted class of an input.

The splits are based on the Gini's diversity index (GDI) [38]. This metric measures the node impurity. The lower the GDI, the better the split. For a data set S at node M, the GDI is defined as:

$$\mathrm{GDI(S)} = 1 - \sum_{k=1}^{K}\left[p_k(x)\right]^2, \tag{6}$$

where K is the number of predefined classes, $p_k(x)$ is the relative frequency [36] of class k at node M defined as:

$$p_k(x) = \frac{1}{N}\sum_{s_k \in S} I(x), \tag{7}$$

where s_k is the number of data points in class k, I is the indicator function, and N is the total number of data points in S at node M.

The number of features selected, at random, is also calculated for each split. The advantage of using a limited number of features is that

it helps to decorrelate trees since strong predictors will not appear in every tree. The minimum node size is one and the number of features at each node is:

$$m = \left\lfloor \sqrt{v} \right\rfloor, \tag{8}$$

where v is the number of features and $\lfloor \cdot \rfloor$ denotes the floor operator.

Now using the m features at each split, pick the best variable/split point [see Eq. 6] and split the node into two daughter nodes. The process is repeated until a node has one class, which corresponds to a GDI of zero.

The random forest classifier creates multiple decision trees by using separate bootstrapped [38] samples from the data for each tree. Bootstrapping also helps to ensure that the trees developed are not correlated. Data not used to train a tree is known as being "out-of-bag". This data is used to evaluate the performance of the classifier.

Bootstrapping is sampling a data set of independent data with replacement. For each bootstrap, z^{*b}, bootstrapping is defined as:

$$z^{*,b} = \left(x_1^*, x_2^*, \ldots, x_N^*\right), \quad b = 1, 2, \ldots B, \tag{9}$$

where b is the bth bootstrap data set for N data points and B is the total number of bootstrapped samples.

After forming the binary trees, a "vote" from each tree determining the class of the "out-of-bag" data is computed by taking into account only data samples that were not used in any decision trees. To form a decision, we let $\hat{C}_b(x)$ be the class prediction of the bth random forest tree, then the final classification prediction is:

$$C_{final}(x) = majority\ vote\left\{\hat{C}_b(x)\right\}^B, \tag{10}$$

where *majority vote* is the class that has the most "votes" from the random forest consisting of B trees.

4. 3D Optical Phase Code Authentication

Twenty speckle patterns were recorded from 3D optical phase code A, B, and C at distances of 30 mm, 70 mm, 110 mm, and 150 mm from the CCD sensor [see Section 2]. In total, there were 12 classes, as described in Table 2, and 120 true class images. Feature extraction was then performed [see Eqs. 1-5] and the random forest classifier was used to authenticate these speckles. Fig. 5 below depicts an overview of the proposed authentication system. The random forest classifier was trained using ten speckles from each class while the other ten were used for testing. The random forest classifier training model was evaluated by calculating the out-of-bag error for the random forest using 100 trees, shown in Fig. 6. After 100 trees, the percent error was about 0.67%.

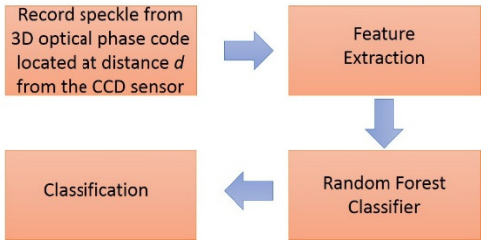

Fig. 5. Overview of the 3D optical phase code authentication system.

Testing data was then inputted into the model using the other ten recorded speckles from each class. We note that the classifier automatically places the data into a class. To determine the reliability of a measurement, we also observe the score that the random forest calculates. The score is the percentage of "votes" from each binary tree to each class. There was a 100% correct classification rate for each class. In addition, the number of votes to the correct class in the proposed classification scheme was on average 99.953%. Thus, the proposed classification scheme may be used to authenticate a unique 3D optical phase mask.

Table 2. A 12 class system was developed using 3D optical phase codes (OPC) A, B, and C and placing the 3D codes at different distances from the CCD sensor.

	3D OPC A	3D OPC B	3D OPC C
30 mm	Class 1	Class 2	Class 3
70 mm	Class 4	Class 5	Class 6
110 mm	Class 7	Class 8	Class 9
150 mm	Class 10	Class 11	Class 12

A test was also conducted to determine the performance of the classifier to speckles from 3D OPCs that do not fall into any classes, which we consider false class data. Fifty speckles were captured from different configurations of 3D OPCs, which were constructed using a process similar to those constructed in Fig. 1, and placed at arbitrary distances from the CCD sensor. Features were extracted from the recorded speckle pattern and inputted into the random forest classifier. If a speckle pattern did not have a 95% vote, it was assumed that the classifier was unable to decide the class of the speckle. An example of a false class speckle pattern is shown in Fig. 7. The false class pattern was created by placing 3D optical phase code C 100 mm from the CCD and recording the resulting speckle pattern. For this particular false class speckle, the classifier determined that the pattern belonged to class 8. Moreover, the score received only 84% of the votes thus we could not determine the veracity of the phase mask and conclude that it was not authentic. Table 3. shows the confusion matrix of the classifier accounting for both true and false class data.

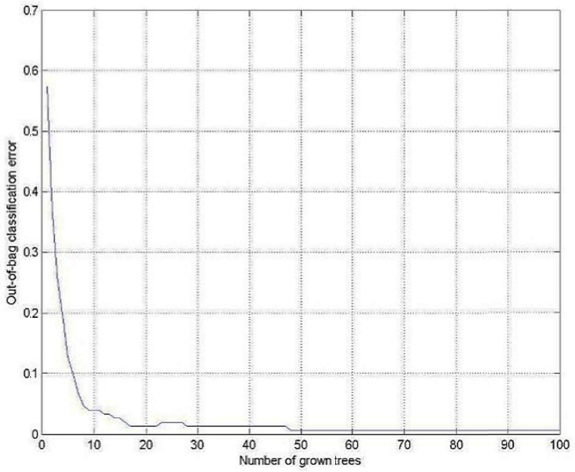

Fig. 6. Out-of-bag classification error using 100 trees which converges to about 0.0067.

Table 3. Classification results for the 12 class system for when 120 test images were used and 50 false class images

		Predicted Class	
		True	False
Actual Class	True	120	0
	False	0	50

The accuracy of the classifier when the 3D OPC was shifted from their original positions was also evaluated. At distances of 70 mm, 110 mm, and 150 mm, 3D optical phase code A was displaced up to +/- 10 mm from the original position by increments of 1 mm. As the 3D optical phase code was further from the CCD device, the classifier was less sensitive to displacement errors as shown in Fig. 8. We note that the classifier was able to correctly classify speckles for all displacements about 110 mm and 150 mm; however, at 70 mm there were misclassifications at – 9 mm and – 10 mm. Thus, a user must be mindful the distance the 3D optical phase code is from the CCD sensor.

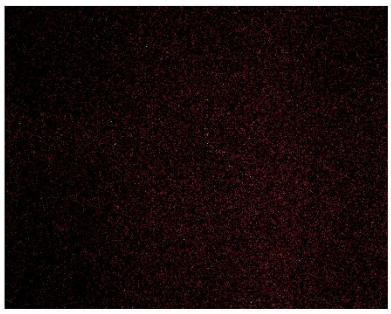

Fig. 7. A false class speckle pattern obtained by placing 3D optical phase code C 100 mm from the CCD sensor.

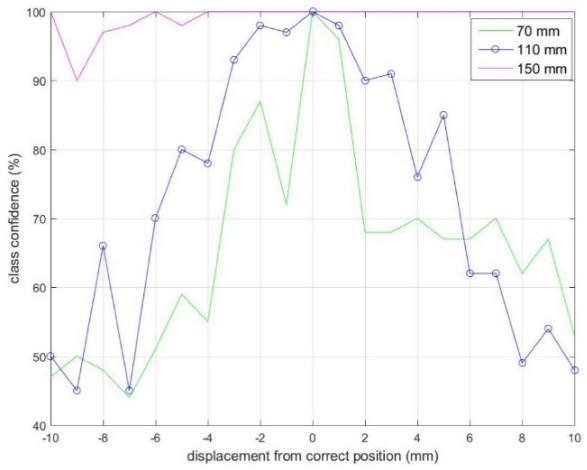

Fig. 8. Effect of displacement of 3D optical phase code A on the class confidence score output from the random forest classifier for distances 70 mm, 110 mm, and 150 mm from the CCD sensor.

5. Conclusion

In conclusion, we present an authentication scheme using a transparent QR code containing a 3D optical phase mask to generate a 3D optical phase code (OPC). An advantage of a 3D optical phase mask over a 2D is that it is difficult to mathematically characterize a 3D code made of randomly scattering medium and/or to duplicate it physically. An optical authentication system was designed using 3 separate 3D OPCs which were placed 30 mm, 70 mm, 110 mm, and 150 mm from a CCD sensor. A 445 nm blue laser diode illuminated the 3D OPCs at each distance to generate a unique speckle pattern that was captured by the CCD. Feature extraction was then performed on the speckle pattern by calculating the mean, variance, skewness, kurtosis, and entropy. A multiclass random forest classifier was used to classify the recorded speckles at each distance. A 100% accuracy rate was achieved. Thus, we have shown we can use mean, variance, skewness, kurtosis and entropy of a speckle image combined with the random forest classifier to determine the authenticity of a 3D OPC. Overall, it is difficult to reproduce the 3D optical code from either the resulting speckle pattern or visual inspection. As a result, we can use this 3D optical phase code system to authenticate an object.

Funding Information. A. Carnicer acknowledges support from Ministerio de Economía y Competitividad (Spain) projects FIS2013-46475-C3-2-P.

Acknowledgment. B. Javidi and A. Markman would like to acknowledge Honeywell for support.

References

1. P. Refregier and B. Javidi, "Optical image encryption based on input plane and Fourier plane random encoding," Opt. Lett. **20**, 767-769 (1995).
2. W. Chen, B. Javidi and X. Chen, "Advances in optical security systems," Adv. Opt. Photon. **6**, 120-155 (2014).
3. T. Naughton, B. Hennelly, and T. Dowling, "Introducing secure modes of operation for optical encryption," J. Opt. Soc. Am. A **25**, 2608 (2008).
4. A. Carnicer, M. Montes-Usategui, S. Arcos and I. Juvells, "Vulnerability to chosen-cyphertext attacks of optical encryption schemes based on double random phase key," Opt. Lett. **30**, 1644-1646 (2005).
5. Y. Frauel, A. Castro, T. Naughton and B. Javidi, "Resistance of the double random phase encryption against various attacks," Opt. Express **15**, 10253-10265 (2007).
6. O. Matoba and B. Javidi, "Encrypted optical memory system using three-dimensional keys in the Fresnel domain," Opt. Lett. **24**, 762-764 (1999).
7. P. Kumar, J. Joseph and K. Joseph, "Optical image encryption using a jigsaw transform for silhouette removal in interference-based methods and decryption with a single spatial light modulator," Appl. Opt. **50**, 1805-1811 (2011).
8. O. Matoba and B. Javidi, "Encrypted optical storage with wavelength-key and random phase codes," Appl. Opt. **38**, 6785-6790 (1999).
9. X. Tan, O. Matoba, Y. Okada-Shudo , M. Ide , T. Shimura and K. Kuroda, "Secure Optical Memory System with Polarization Encryption" Appl. Opt. **40**, 2310-2315 (2001).
10. J. Heanue, M. Bashaw and L. Hesselink, "Encrypted holographic data storage based on orthogonal-phase-code multiplexing," Appl. Opt. **34**, 6012-6015 (1995).
11. M. Toishi, M. Hara, K. Tanaka, T. Tanaka and K. Watanabe, "Novel Encryption Method Using Multi Reference Patterns in Coaxial Holographic Data Storage," Jpn. J. Appl. Phys. 46, 3775-3781 (1995).
12. B. Javidi and T. Nomura, "Securing information by use of digital holography," Opt. Lett. **25**, 28-30 (2000).
13. K. Nakano, M. Takeda, H. Suzuki, and M. Yamaguchi, "Evaluations of phase-only double random phase encoding based on key-space analysis," Appl. Opt. **52**, 1276-1283 (2013).
14. E. Tajahuerce and B. Javidi, "Encrypting three-dimensional information with digital holography," Appl. Opt. **39**, 6595-6601 (2000).
15. H. Tashima, M. Takeda, H. Suzuki, T. Obi, M. Yamaguchi, and N. Ohyama, "Known plaintext attack on double random phase encoding using fingerprint as key and a method for avoiding the attack," Opt. Express **18**, 13772–13781 (2010).

16. O. Matoba, T. Sawasaki and K. Nitta, "Optical authentication method using a three-dimensional phase object with various wavelength readouts," Appl. Opt **47**, 4400-4404 (2008).
17. B. Javidi and T. Nomura, "Polarization encoding for optical security systems," Opt. Eng. **39,** 2439-2443 (2000).
18. S. Rajput and N. Nishchal, "An optical encryption and authentication scheme using asymmetric keys," J. Opt. Soc. Am. A **31**, 1233-1238 (2014).
19. A. Markman, B. Javidi and M. Tehranipoor, "Photon-Counting Security Tagging and Verification Using Optically Encoded QR Codes," IEEE J. Photonics **6**, 1-9 (2014).
20. A. Carnicer, O. Arteaga, E. Pascual, A. Canillas, S. Vallmitjana-Rico, B. Javidi, and E. Bertran, "Optical security verification by synthesizing thin films with unique polarimetric signatures," Opt. Lett. **40**, 5399-5402 (2015).
21. A. Carnicer, A. Hassanfiroozi, P. Latorre-Carmona, Y. Huang and B. Javidi, "Security authentication using phase-encoded nanoparticle structures and polarized light," Opt. Lett. **40**, 135-138 (2015).
22. E. Pérez-Cabré, H. Abril, M. Millán, and B. Javidi , "Photon-counting double-random-phase encoding for secure image verification and retrieval," J. Opt. **14**, 094001 (2012).
23. A. Markman and B. Javidi, "Full-phase photon-counting double-random-phase encryption," J. Opt. Soc. Am. A **31**, 394-403 (2014).
24. S. Kishk and B. Javidi, "3D object watermarking by a 3D hidden object, Opt. Express **11**, 874-888 (2003).
25. A. Shortt, T. Naughton, and B. Javidi, "Histogram approaches for lossy compression of digital holograms of three-dimensional objects," IEEE Trans. Image Process. **16**, 1548-1556 (2007).
26. O. Matoba, S. Matsuki, and K. Nitta, "Secure data storage by three-dimensional absorbers in highly scattering volume medium," JPCS **139**, 1-5 (2008).
27. U. Guler and R. Turan, "Effect of particle properties and light polarization on the plasmonic resonances in metallic nanoparticles," Opt. Express **18**, 17322-17338 (2010).
28. B. Canfield, S. Kujala, K. Jefimovs, J. Turunen and M. Kauranen, "Linear and nonlinear optical responses influenced by broken symmetry in an array of gold nanoparticles," Opt. Express 12, 5418-5423 (2004).
29. S. Goorden, M. Horstmann, A. Mosk, B. Škorić and P. Pinkse, "Quantum-secure authentication of a physical unclonable key," Optica 1, 421-424 (2014).
30. J. Goodman, Introduction to Fourier optics (McGraw-Hill, 2004).
31. J. Goodman, Statistical optics (Wiley, 2000).
32. J.C. Dainty, "The statistics of speckle patterns," Progress in optics 14, 1-46 (1977).
33. D. Sheskin, Handbook of parametric and nonparametric statistical procedures (CRC Press, 1997).
34. Tsinaslandis and Zapranis, Technical Analysis for Algorithmic Pattern Recognition, (Spring, 2015).
35. T. Cover and J. Thomas, Elements of information theory (Wiley, 1991).
36. R. Gonzalez and P. Wintz, Digital image processing (Addison-Wesley, 1987).
37. K. Black, Business statistics (Wiley, 2008).
38. M. Kantardzic, Data Mining: Concepts, Models, Methods, and Algorithms, 2nd Edition (Wiley, 2011).
39. L. Breiman , "Random forests," Mach. Learn. 45, 5-32 (2001).